Description of a ray trace algorithm for the evaluation of pump power absorption in double-clad fibers

Roberto NARRO-GARCÍA*, Eugenio RODRÍGUEZ, Luis PONCE, Eduardo DE POSADA,
Teresa FLORES, Miguel ARRONTE

Laboratorio de Tecnología Láser, CICATA-IPN Unidad Altamira,
km 14.5 Carretera Tampico-Puerto Industrial Altamira, Altamira 89600, TAMPS, México

*Corresponding author: robert_ng@hotmail.com

An algorithm for the analysis of the double-clad fiber design is presented. The algorithm developed in the MATLAB computing language, is based on ray tracing method applied to three-dimensional graphics figures which are composed of a set of planes. The algorithm can evaluate an arbitrarily large number of ray paths calculating the corresponding pump absorption in each of the fiber elements according to the Lambert–Beer law. The beam path is evaluated in three dimensions considering the losses by reflection and refraction both at the fiber faces and within the fiber. Due to its flexibility, the algorithm can be used to study the ray propagation in double-clad fiber with: *i*) variable geometries of the inner clad and the core; *ii*) different position of the core inside the inner clad; and *iii*) bending and tapper effects.

Keywords: ray trace method, ray trace algorithm, pumps absorption, double-clad fiber.

1. Introduction

Power scaling in conventional rare-earth-doped mono-mode fibers is limited because of the poor coupling efficiency from multi-mode diode laser arrays to the single-mode core of the fiber. To increase the coupling efficiency, one possible solution is increasing fiber diameter and numerical aperture for better matching with the high power pumping diode laser. However, an increased fiber diameter leads to multi-mode operation and reduced beam quality. To overcome these problems, double-clad fibers have been developed [1, 2]. With this technique the pump radiation is not directly pumped into the doped fiber core but rather into a large surrounding multi-mode waveguide with a high numerical aperture. This enables an efficient coupling of the high-power diode laser to the fiber. The pump light is gradually coupled into the active mono-mode core where it is absorbed. This method provides a simple and efficient means to convert multi-mode light from the high-power pumping diode laser into laser radiation with excellent beam quality [3–5]. In this case, the maximal output

power of the single-mode double-clad fiber laser is limited by the power of the pump and the efficiency of the pumping absorption in the core [6, 7].

The pumping absorption has been experimentally studied and also numerically simulated by several authors in double-clad fibers, assuming that, among other factors, it is proportional to the number of light "rays" crossing the fiber core.

It is well known that fibers with cylindrical geometry (core at the fiber center), exhibit poor performance because the helical rays miss the core and only the meridional rays are absorbed [8–10]. Previous reports have shown that a greater efficiency of the pumping absorption in double-clad optical fibers can be achieved by varying: *i*) the position of the core inside the circular inner clad [11, 12]; or *ii*) the geometry of the inner clad cross-section [13–16].

Based on 2D and 3D analysis, Anping and Kenichi [11] demonstrated that the efficiency of pumping absorption in double-clad fibers with off-center core or rectangular inner clad can be up to four times greater than the efficiency of the pumping absorption in fibers with circular inner clad and core in the geometric center of the fiber. It is worth mentioning that this research did not take into account the presence of the core nor the losses due to reflection because the fiber cores they considered were very small (6, 12 and 24 µm) in comparison with the clad (400 µm). Moreover, the results of the 3D analysis were only presented for fibers with circular inner clad.

Based on the geometrical optics approximation, Konieczny *et al*. [12] established a comparison between a circular geometry, an off-center geometry and a D-type inner clad. For the off-center geometry (fiber core 5–7 µm, fiber length 2 m; and absorption coefficient of the core region 100 dB/m), they reported that the pump power absorption reaches the maximum (around 12%) when the site of the active core is shifted off from the fiber center symmetry about 32 µm.

On the other hand, Philippe Leproux *et al*. [15] reported that a constant absorption coefficient can be achieved along the fiber regardless of the pumping conditions when using a chaotic type inner clad. Gorjan *et al*. [16] using a double-clad, 4 m long fiber with D-type inner clad, obtained experimentally 99% efficiency of the pumping absorption (the resulting value of the absorption coefficient of the core region was 1.6 mm^{-1}).

More recently, Witkowski and Grobelny [17] reported another technique to describe the pumping absorption. The algorithm is based on ray tracing method and was extended to analyze both the scattering and the pulse shape along the fiber. Although it is a 3D analysis and considers the case of graded index fibers, it only shows results for fibers with circular inner clad, moreover, it is not clear how this algorithm could be applied to the treatment of fibers with variable inner clad geometry.

In this paper, we present the description of an algorithm for the study of double clad fibers which allows the simulation of a large number of rays traveling along the fiber as well as its absorption according to Lambert–Beer law. The beam path is evaluated in three dimensions considering the losses by reflection and refraction at the faces and within the fiber. The algorithm is based on the design of the fiber as a group of 3D objects using a computer aided design program (3D Studio Max); each

object is decomposed into small triangular planes, which simplifies the problem of finding the intersection of the beam with each object in the fiber. The algorithm also considers the presence of the fiber core, *i.e.*, it makes the corresponding deviations of the beam path according to the laws of reflection and refraction when it crosses the fiber core.

Due to its flexibility, the algorithm can be used to study the ray propagation in double-clad fibers with: *i*) variable geometries of the inner clad and the core; *ii*) different position of the core inside the inner clad; and *iii*) bending and taper effects.

2. Description of the numerical algorithm

This algorithm is used to describe the path of the pump beam within a double-clad optical fiber. To simplify the description of the algorithm only the beam path in the inner clad and the core of the fiber will be considered. The fiber is divided into two objects "clad" and "core", each one of them comprises n planes and in turn each plane is represented by three points in space (as shown in Fig. 1):

$$\text{Objects} = \{\text{Clad, Core}\}$$

$$\text{Clad} = \{F_1, F_2, F_3, ..., F_n\}$$

$$\text{Core} = \{N_1, N_2, N_3, ..., N_n\} \tag{1}$$

$$\text{Fi} = \{P_{i,1}(x_1, y_1, z_1), P_{i,2}(x_2, y_2, z_2), P_{i,3}(x_3, y_3, z_3)\}$$

For the design of the fiber it is recommended to use a CAD (computer aided design) program which facilitates the fiber design in 3D and allows exporting the design into
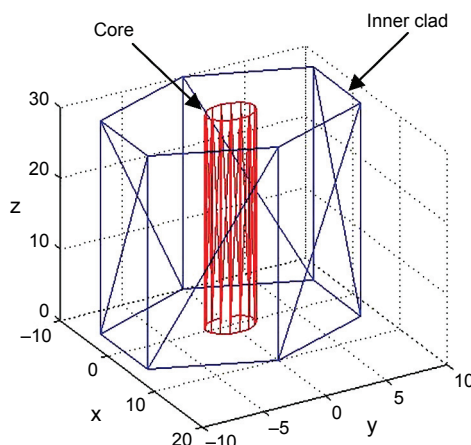

Fig. 1. Schematic representation of a 3D fiber showing the core and the inner clad. The inner clad exhibits hexagonal geometry comprising 12 triangular planes. The core exhibits circular geometry (polygon of 18 sides) and is formed by 32 triangular planes.

T a b l e 1. Information regarding planes that make up the fiber.

| | | P_1 | | | P_2 | | | P_3 | |
Plane	x_1	y_1	z_1	x_2	y_2	z_2	x_3	y_3	z_3
1	$x_1(1)$	$y_1(1)$	$z_1(1)$	$x_2(1)$	$y_2(1)$	$z_2(1)$	$x_3(1)$	$y_3(1)$	$z_3(1)$
2	$x_1(2)$	$y_1(2)$	$z_1(2)$	$x_2(2)$	$y_2(2)$	$z_2(2)$	$x_3(2)$	$y_3(2)$	$z_3(2)$
3	$x_1(3)$	$y_1(3)$	$z_1(3)$	$x_2(3)$	$y_2(3)$	$z_2(3)$	$x_3(3)$	$y_3(3)$	$z_3(3)$
n	$x_1(n)$	$y_1(n)$	$z_1(n)$	$x_2(n)$	$y_2(n)$	$z_2(n)$	$x_3(n)$	$y_3(n)$	$z_3(n)$

T a b l e 2. Information on the objects comprising the fiber and also the planes conforming to each object.

Object	Initial	Final
Core	1	32
Clad	33	44
Space	45	56

a set of two tables of values. The first one contains information regarding the planes that make up the fiber including the respective coordinates of its vertices (P_1, P_2, P_3) as shown in Tab. 1. A second table is also generated indicating the objects comprising the fiber and also the planes conforming each object (Tab. 2). The second table shows, for example, that the fiber is composed of the objects "core" and "clad", indicating both the initial and final plane which conform to each one of these objects.

Additionally, we have included a third object called "space", the latter may be a prism that surrounds the fiber, so that every time a ray intersects this object, it means that the light beam came out of the fiber indicating the program must stop.

Below, the steps of ray tracing are summarized, which are described in detail in the following sections:
   – Calculate the intersection point (x_f, y_f, z_f) of the ray with each plane;
   – Select the plane of intersection and distance traveled by the beam;
   – Select the refractive index and absorption coefficient;
   – Determine the angle of reflection and refraction;
   – Determine the direction of the reflected and refracted ray;
   – Evaluate the losses by reflection and refraction;
   – Determine the absorption of the beam through the fiber according to the Lambert–Beer law;
   – Calculate the following ray.

2.1. Calculating the intersection point of the ray with the plane

Let us consider the ray which travels through the point $P_i = (x_i, y_i, z_i)$ to $P_f = (x_f, y_f, z_f)$. This ray is parallel to the vector $\mathbf{P_i P_f} = (A, B, C)$. The parametric equation for this ray is:

$$x = (Au) + x_i \tag{2}$$

$$y = (Bu) + y_i \tag{3}$$

$$z = (Cu) + z_i \tag{4}$$

$$u \in R \tag{5}$$

If F_i is the plane containing the point $P_3 = (x_3, y_3, z_3)$ whose normal vector is $\mathbf{V_n} = (a, b, c)$, then the Cartesian equation for F_i, is:

$$ax_3 + by_3 + cz_3 + d = 0 \tag{6}$$

$$d = -ax_3 - by_3 - cz_3 \tag{7}$$

Substituting Eqs. (2)–(4) in Eq. (6) and solving for u_f we obtain:

$$a(Au_f + x_i) + b(Bu_f + y_i) + c(Cu_f + z_i) + d = 0 \tag{8}$$

$$u_f = -\frac{ax_i + by_i + cz_i + d}{Aa + Bb + Cc} \tag{9}$$

The intersection point coordinates (x_f, y_f, z_f) of the beam with the plane are obtained by substituting Eq. (9) in Eqs. (2)–(4).

$$x_f = (Au_f) + x_i \tag{10}$$
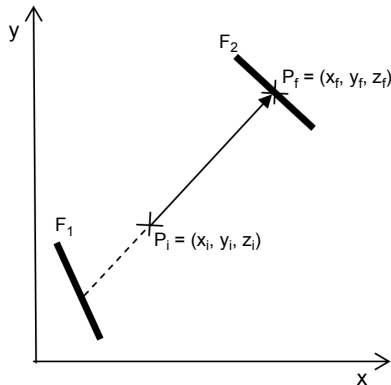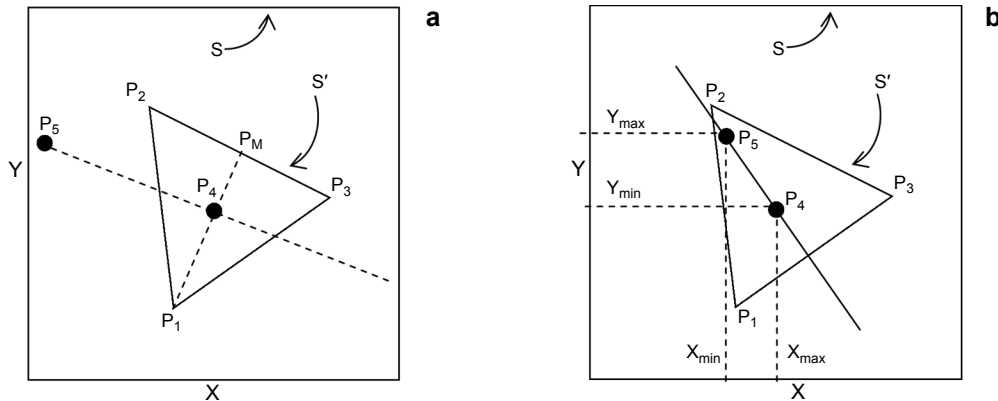
$$y_f = (Bu_f) + y_i \tag{11}$$

$$z_f = (Cu_f) + z_i \tag{12}$$

2.2. Selecting the plane of intersection and distance traveled by the beam

Each time the ray path is calculated, the intersection of that ray with all the planes of Tab. 1 is determined, by using the equations presented in the previous section. With the exception of the planes that are on the same beam path or those which are parallel to it, the beam will intercept all other planes comprising the objects "clad" and "core". In order to determine which plane is the correct one to choose, the following three criteria are established, which should be followed in the sequence presented:

1) The beam direction: The only paths considered are those whose direction is consistent with the direction of the beam. Figure 2 shows a ray that intersects the planes F_1 and F_2, but the direction of the beam shows that the correct plane to choose is the plane F_2. This occurs only when $u_f > 0$ (Eq. (9)).

2) The domain of the plane. The intersection must be within the limits of the plane. Figure 3a shows that S' is a subset of the general plane S and P_5 is a point belonging

Fig. 2. Ray intersection with the planes F_1 and F_2.

Fig. 3. Point P_5 is outside the plane (**a**). Point P_5 is inside the plane (**b**).

to the plane *S*, but it is outside the domain of the plane *S′*. The algorithm to determine whether a point is within the domain of the plane is the following:

– Transforming the system to be evaluated in two dimensions.

– Determining a point within the domain of the plane (P_4 in Fig. 3**a**). This point can be calculated by determining the midpoint of the line P_1P_M, where P_M is the midpoint of the line P_2P_3.

– Determining the intersection of the straight line P_4P_5 with the lines P_1P_2, P_1P_3 and P_2P_3, respectively, as shown in Fig. 3**b**. In the case presented in Fig. 3**b**, the intersection with the line P_2P_3 is ruled out because it lies outside the domain of the line.

– Point P_5 is within the domain of the plane *S′* if:

$$\left\{(X_5 \geq X_{\min}) \quad \text{AND} \quad (X_5 \leq X_{\max})\right\} \quad \text{AND} \quad \left\{(Y_5 \geq Y_{\min}) \quad \text{AND} \quad (Y_5 \leq Y_{\max})\right\} \tag{13}$$

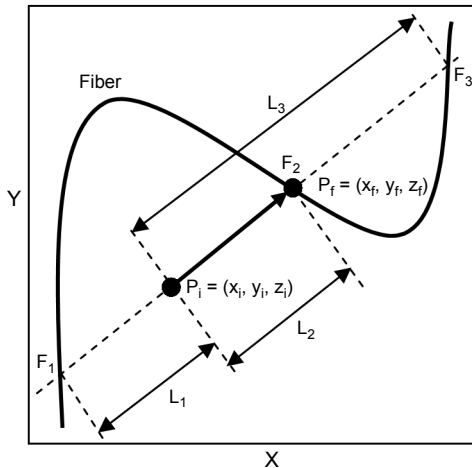– Return the system to three dimensions.

Fig. 4. Example of a ray intersecting several planes in a bent fiber.

3) The distance traveled L:

$$L = \left[(x_f - x_i)^2 + (y_f - y_i)^2 + (z_f - z_i)^2 \right]^{1/2} \tag{14}$$

In the event the fiber is bent, as shown in Fig. 4, the beam intersects planes F_2 and F_3 which are in the beam direction and within the domain. In this case, the plane closer to the starting position of the beam should be selected. In the example, the minimum distance the beam travels is L_1, but this plane was discarded by criterion (1), therefore the minimum distance is L_2 corresponding to the intersection with plane F_2.

2.3. Selecting the refractive index and the absorption coefficient

Once the plane intersected by the beam is known, by means of Tab. 2, it is determined to what object this plane belongs. If the beam was initially propagating through the core ($M_1 = C$) and it intersects the Object = {Core}, then the refractive index of medium 1 is equal to the index of the core ($n_1 = C$). The refractive index of medium 2 is the index of the inner clad ($n_2 = C$), the absorption coefficient is the one corresponding to the core ($\alpha = C$) and the refracted beam propagates through the inner

T a b l e 3. Logic for selecting the refractive index and absorption coefficient. C – core; IC – internal clad, EC – external clad; OF – final object; M_1 – medium 1 and M_2 – medium 2; α – absorption coefficient of the initial medium.

M_1	OF	n_1	n_2	α	M_2
C	C	C	IC	C	IC
IC	C	IC	C	IC	C
IC	IC	IC	EC	IC	IC

clad (M_2 = IC). This is shown in Tab. 3 together with the two other possibilities that may occur in the example that has been explained in this work.

By evaluating the pure reflection of the ray, it is assumed that each bundle propagating through a medium remains on the same medium after all reflections, *i.e.*, $M_1 = M_2$ = medium of the object and α = absorption coefficient of the initial medium.

2.4. Determining the angle of reflection and refraction

Figure 5 shows the general schematic representation of reflection and refraction when a beam crosses the boundary between two media of different refractive indices (n_1, n_2). In general, part of the incident beam (V_i) is reflected in the direction V_r and part of it is transmitted to the second medium in the direction V_t. However, for $n_1 > n_2$ there is a certain critical angle ($\theta_c = \mathrm{asin}(n_2/n_1)$), above which the incident beam is totally reflected to the medium with the higher refractive index n_1.
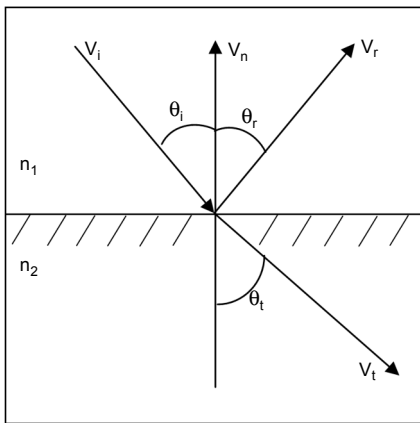

Fig. 5. Schematic representation of the reflection and refraction of a beam crossing the boundary surface between two media of different refractive indices n_1 and n_2. V_n is the normal vector to the surface. V_i, V_r and V_t are the incidence, reflected and transmitted vectors, respectively. θ_i, θ_r and θ_t are the incidence, reflection and refraction angles, respectively, and all of them are measured relative to the surface normal.

The algorithm presented in this report, evaluates the percentage of the beam reflected and refracted each time the beam reaches the boundary of a different medium (Object = {Clad, Core}). Having once determined the intersection point $P_f(x_f, y_f, z_f)$ of the beam with the proper plane of incidence, the algorithm proceeds to calculate the incidence vector V_i in its contrary direction from the initial and final coordinates (see Fig. 5)

$$V_i = ((x_i - x_f), (y_i - y_f), (z_i - z_f)) \tag{15}$$

The angle of reflection is the same as the angle of incidence formed by the incidence vector (V_i) and the normal to the plane (V_n). This angle can be calculated according to the relation:

$$\theta_i = \cos^{-1}\left(\frac{V_i \bullet V_n}{|V_i||V_n|}\right) \tag{16}$$

The program compares the incidence angle with the critical angle to determine whether the beam is totally reflected or part of it is refracted to the second medium. In the latter case, the refraction angle is obtained from Snell's law (Eq. (17)) using the refractive indices presented in Tab. 3

$$\theta_t = \sin^{-1}\left(\frac{n_1 \sin \theta_i}{n_2}\right) \tag{17}$$

2.5. Determining the direction of the reflected ray

In order to determine the direction of the beam reflected by any plane comprising the fiber, the following transformations are performed: firstly, the matrix T transfers the origin of coordinates to the intersection point of the incidence vector R_i with the plane F_j. Successive rotations around the x-axis (R_x) and the y-axis (R_y) align the z-axis with the vector normal to plane F_i. At this point, the F_{xy} matrix produces the reflection of the incidence vector with respect to "x" and "y" axes. Finally, by inverse transformations the "x" and "y" axes are rotated and the origin of coordinates is transferred to their original position, respectively.

The total transformation matrix for the reflection (MTR) is presented as a product of matrices (transfer matrix T, rotation matrix "x" R_x, rotation matrix "y" R_y, inverse transfer matrix T^{-1}, inverse rotation matrix "x" R_x^{-1}, inverse rotation matrix "y" R_y^{-1}, reflection matrix F_{xy}, ray matrix R_i), where each matrix performs partial transformations to the vector R_i:

$$\text{MTR} = R_i\, T\, R_x\, R_y\, F_{xy}\, R_x^{-1}\, R_y^{-1}\, T^{-1} =$$

$$= \begin{bmatrix} (1,1) & (1,2) & (1,3) & (1,4) \\ (2,1) & (2,2) & (2,3) & (2,4) \end{bmatrix} \tag{18}$$

where: $T = \begin{bmatrix} 1 & 0 & 0 & 0 \\ 0 & 1 & 0 & 0 \\ 0 & 0 & 1 & 0 \\ -x_f & -y_f & -z_f & 1 \end{bmatrix}$, $R_x = \begin{bmatrix} 1 & 0 & 0 & 0 \\ 0 & c/\Gamma & b/\Gamma & 0 \\ 0 & -b/\Gamma & -c/\Gamma & 0 \\ 0 & 0 & 0 & 1 \end{bmatrix}$, $R_y = \begin{bmatrix} \Gamma/H & 0 & a/H & 0 \\ 0 & 1 & 0 & 0 \\ -a/H & 0 & \Gamma/H & 0 \\ 0 & 0 & 0 & 1 \end{bmatrix}$,

$$T^{-1} = \begin{bmatrix} 1 & 0 & 0 & 0 \\ 0 & 1 & 0 & 0 \\ 0 & 0 & 1 & 0 \\ x_f & y_f & z_f & 1 \end{bmatrix}, \quad R_x^{-1} = \begin{bmatrix} 1 & 0 & 0 & 0 \\ 0 & c/\Gamma & -b/\Gamma & 0 \\ 0 & b/\Gamma & c/\Gamma & 0 \\ 0 & 0 & 0 & 1 \end{bmatrix}, \quad R_y^{-1} = \begin{bmatrix} \Gamma/H & 0 & -a/H & 0 \\ 0 & 1 & 0 & 0 \\ a/H & 0 & \Gamma/H & 0 \\ 0 & 0 & 0 & 1 \end{bmatrix},$$

$$F_{xy} = \begin{bmatrix} -1 & 0 & 0 & 0 \\ 0 & -1 & 0 & 0 \\ 0 & 0 & 1 & 0 \\ 0 & 0 & 0 & 1 \end{bmatrix}, \quad R_i = \begin{bmatrix} x_f & y_f & z_f & 1 \\ x_i & y_i & z_i & 1 \end{bmatrix}, \quad \text{and} \quad H = \left(a^2 + b^2 + c^2 \right)^{1/2},$$

$$\Gamma = \left(b^2 + c^2 \right)^{1/2}.$$

The reflected beam direction is obtained from MTR (Eq. (18)) as follows:

$$A = \text{MTR}(2, 1) - \text{MTR}(1, 1) \tag{19}$$

$$B = \text{MTR}(2, 2) - \text{MTR}(1, 2) \tag{20}$$

$$C = \text{MTR}(2, 3) - \text{MTR}(1, 3) \tag{21}$$

2.6. Determining the direction of the refracted beam

In a similar manner as described by the reflection, the origin of coordinates is transferred to the intersection point of the incidence vector R_i with the plane F_i through the transfer matrix T. Successive rotations around the *x*-axis (R_x) and the *y*-axis (R_y) align the *z*-axis with the vector normal to plane F_i. At this point, the reflection of the incidence vector with respect to "*x*" and "*y*" axes is calculated according to:

$$\text{MTT}_1 = R_i\, T\, R_x\, R_y\, F_{xy} = \begin{bmatrix} (1, 1) & (1, 2) & (1, 3) & (1, 4) \\ (2, 1) & (2, 2) & (2, 3) & (2, 4) \end{bmatrix} \tag{22}$$

Taking into account that both the reflected and the refracted beam are in the same plane, the matrix element $\text{MTT}_1(2, 3)$ should be modified according the algorithm presented in Fig. 6.

After calculating the *z* coordinate of the refracted ray, through inverse transformations the "*x*" and "*y*" axes are rotated and the origin of coordinates is transferred to their original position, respectively. Thus the transformation matrix for refraction is:

$$\text{MTT}_2 = \text{MTT}_1\, R_y^{-1}\, R_x^{-1}\, T^{-1} = \begin{bmatrix} (1, 1) & (1, 2) & (1, 3) & (1, 4) \\ (2, 1) & (2, 2) & (2, 3) & (2, 4) \end{bmatrix} \tag{23}$$
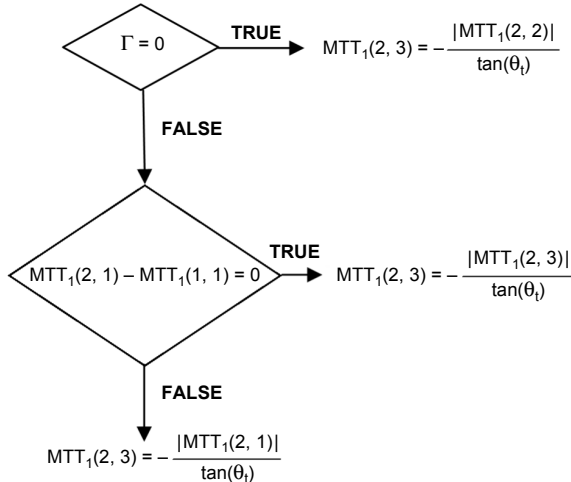
Fig. 6. Algorithm for calculation of the matrix element $MTT_1(2, 3)$.

The directions of the refracted vector are obtained from Eq. (23) as follows:

$$A = MTT_2(2, 1) - MTT_2(1, 1) \tag{24}$$

$$B = MTT_2(2, 2) - MTT_2(1, 2) \tag{25}$$

$$C = MTT_2(2, 3) - MTT_2(1, 3) \tag{26}$$

2.7. Evaluation of losses by reflection and refraction

Fresnel's equations were used to estimate the losses by reflection and refraction. Each time a ray intersects a different plane of the fiber; both the reflection and the transmission coefficients are calculated.

For unpolarized waves propagating through a non-absorbing material the reflection coefficient R is given by [18]:

$$R = \frac{R_s + R_p}{2} \tag{27}$$

where R_s and R_p are the reflection coefficients perpendicular and parallel to the plane of incidence, respectively. According to Fresnel's equations these coefficients can be calculated as follows:

$$R_s = \left[\frac{\sin(\theta_t - \theta_i)}{\sin(\theta_t + \theta_i)} \right]^2 \tag{28}$$

$$R_p = \left[\frac{\tan(\theta_t - \theta_i)}{\tan(\theta_t + \theta_i)} \right]^2 \tag{29}$$

The transmission coefficient T is given by

$$T = 1 - R \tag{30}$$

For commercial fibers, where the difference in the clad-core refractive index is of the order of 10^{-3}, and for fiber lengths of a few meters, the losses by reflection and refraction are very small and insignificant. However, including this feature in the algorithm enables the calculations in long fibers.

Moreover, the algorithm is intended to evaluate the ray propagation in double clad fibers with different inner-clad/core geometries; and also the bending and tapper effects. In these cases, light could strike the core/inner-clad or the inner-clad/external--clad interfaces at angles lower than the critical angle and will be lost into the external clad as illustrated in Fig. 7.

2.8. Simulation examples

To validate the algorithm proposed in this work, the beam path for one ray was calculated within fibers exhibiting two different geometries: axis and a D-shaped symmetry.

For fibers with axis symmetry (Figs. 8**a** and 8**b**), the inner clad and core diameter were 300 and 30 µm, respectively. Moreover, calculations inside these fibers were carried out at two different incidence angles of the pump beam, measured relative to the surface normal.

The surfaces of both the core and the inner clad were approximated to a cylinder comprising a 18-sided and a 200-sided prism[*], respectively. Results show that the rays (blue lines) propagate along the fiber and they never cross the center of symmetry and consequently they are not absorbed by the core. These rays are known as "helical rays" [12] which significantly decrease the pump absorption efficiency in fibers with axis symmetry.

For calculations inside the D-shaped fiber (Fig. 8**c**), the inner clad and core diameter were 350 and 30 µm, respectively. The surfaces of both the core and the D-shaped inner clad were approximated to a cylinders as described above. The 200-sided cylinder, which represents the inner clad, exhibits a rectangular section (cut) along the longitudinal fiber axis. Results show that this ray crosses several times the symmetry center of the inner clad. These rays, known as "meridian rays", can be absorbed inside the core, improving the absorption efficiency in fibers with this kind of geometry.

---

[*]In geometry, a **prism** is a polyhedron with an *n*-sided polygonal base, a translated copy of this base (not in the same plane as the first), and *n* other faces (necessarily all parallelograms) joining corresponding sides of the two bases.
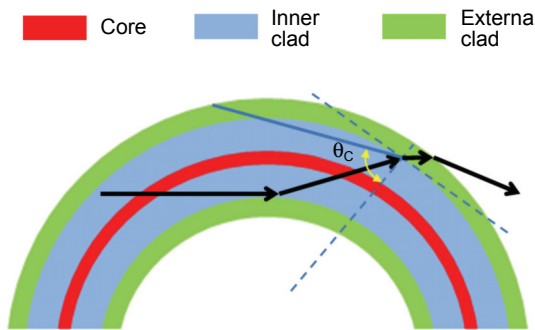
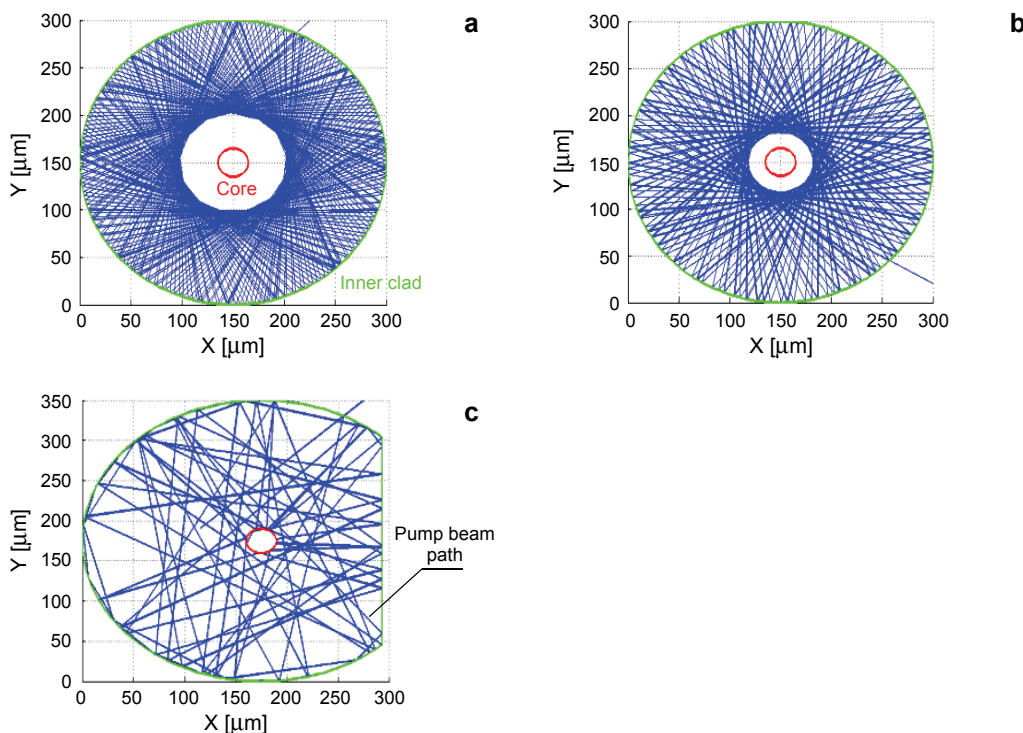Fig. 7. Losses due to macrobending.

Fig. 8. Distribution of the pump beam path inside the inner clad for different fiber cross-sections. Core/clad diameter = 30/300 µm (**a**, **b**); core/clad diameter = 30/350 µm (**c**). In the simulations, we considered the following: core/clad numerical apertures of 0.12/0.5; fiber length = 1 m; the initial rays were coupled to the inner clad; the beam divergence was $\theta = 0.1$ rad; and in all the cases straight fibers were taken into account.

These calculations demonstrate that the approximation of the cylindrical core/clad by triangular surfaces does not avoid the propagation of helical modes, which significantly influence the distribution of pump power in the fiber – decreasing the efficiency of pump absorption in fibers with axis symmetry.

3. Conclusions

In this work, we report an algorithm to describe the beam path within the double-clad optical fibers. The algorithm developed in the MATLAB computing language, is based on ray tracing method that can be applied to three-dimensional graphics figures which are composed of a set of planes. For its treatment the fiber is divided into two objects "clad" and "core", each one of them is composed of n triangular planes. The authors would like to emphasize that the division of the fiber in a set of triangular planes is an easy and novel (concerning the fiber design) method for finding the intersection of the beam with the objects of the fiber. This simplifies the calculations and allows evaluation of different fiber geometries.

In the simulations, conducted both cylindrical and D-shaped fibers reveal the propagation of "helical" and "meridian", respectively. This indicates that the approximation of the cylindrical core/clad by triangular surfaces well describes the fiber geometry for calculations.

The algorithm enables the propagation of a huge number of rays along the fiber, considering the reflection, refraction and absorption of the beam at each point it intercepts a fiber plane. This feature enables the use of the algorithm for calculations in long fibers.

Due to its flexibility, the algorithm can be used to study the ray propagation in double-clad fiber with: *i*) variable geometries of the inner clad and the core; *ii*) different positions and sizes of the core inside the inner clad; and *iii*) bending and tapper effects.

References

[1] SNITZER E., TUMMINELLI R., *SiO$_2$-clad fibers with selectively volatilized soft-glass cores*, Optics Letters **14**(14), 1989, pp. 757–759.
[2] PO H., CAO J.D., LALIBERTE B.M., MINNS R.A., ROBINSON R.F., ROCKNEY B.H., TRICCA R.R., ZHANG Y.H., *High power neodymium-doped single transverse mode fibre laser*, Electronics Letters **29**(17), 1993, pp. 1500–1501.
[3] LIMPERT J., LIEM A., ZELLMER H., TUNNERMANN A., *500 W continuous-wave fibre laser with excellent beam quality*, Electronics Letters **39**(8), 2003, pp. 645–647.
[4] LEE Y.W., SINHA S., DIGONNET M.J.F., BYER R.L., JIANG S., *20 W single-mode Yb^{3+}-doped phosphate fiber laser*, Optics Letters **31**(22), 2006, pp. 3255–3257.
[5] FILIPPOV V., CHAMOROVSKII Y., KERTTULA J., KHOLODKOV A., OKHOTNIKOV O.G., *600 W power scalable single transverse mode tapered double-clad fiber laser*, Optics Express **17**(3), 2009, pp. 1203–1214.
[6] HE X., OVTCHINNIKOV A., YANG S., HARRISON J., FEITISCH A., *Efficient high power reliable InGaAs/AlGaAs (940 nm) monolithic laser diode arrays*, Electronics Letters **35**(20), 1999, pp. 1739–1740.
[7] DOMINIC V., MACCORMACK S., WAARTS R., SANDERS S., BICKNESE S., DOHLE R., WOLAK E., YEH P.S., ZUCKER E., *110 W fibre laser*, Electronics Letters **35**(14), 1999, pp. 1158–1160.

[8] MINELLY J.D., BARNES W.L., LAMING R.I., MORKEL P.R., TOWNSEND J.E., GRUBB S.G., PAYNE D.N., *Diode-array pumping of Er^{3+}/Yb^{3+} Co-doped fiber lasers and amplifiers*, IEEE Photonics Technology Letters **5**(3), 1993, pp. 301–303.

[9] ZELLMER H., WILLAMOWSKI U., TÜNNERMANN A., WELLING H., UNGER S., REICHEL V., MÜLLER H.-R., KIRCHHOF J., ALBERS P., *High-power cw neodymium-doped fiber laser operating at 9.2 W with high beam quality*, Optics Letters **20**(6), 1995, pp. 578–580.

[10] BEDÖ S., LÜTHY W., WEBER H.P., *The effective absorption coefficient in double-clad fibres*, Optics Communications **99**(5–6), 1993, pp. 331–335.

[11] ANPING L., KENICHI U., *The absorption characteristics of circular, offset, and rectangular double-clad fibers*, Optics Communications **132**(5–6), 1996, pp. 511–518.

[12] KONIECZNY P., ŚWIDERSKI J., ZAJĄC A., SKÓRCZAKOWSKI M., *Analysis of activation of active double-clad optical fibers*, Optica Applicata **35**(4), 2005, pp. 955–968.

[13] LEPROUX P., FÉVRIER S., DOYA V., ROY P., PAGNOUX D., *Modeling and optimization of double-clad fiber amplifiers using chaotic propagation of the pump*, Optical Fiber Technology **7**(4), 2001, pp. 324–339.

[14] DOYA V., LEGRAND O., MORTESSAGNE F., *Optimized absorption in a chaotic double-clad fiber amplifier*, Optics Letters **26**(12), 2001, pp. 872–874.

[15] LEPROUX P., DOYA V., ROY P., PAGNOUX D., MORTESSAGNE F., LEGRAND O., *Experimental study of pump power absorption along rare-earth-doped double clad optical fibres*, Optics Communications **218**(4–6), 2003, pp. 249–254.

[16] GORJAN M., MARINČEK M., ČOPIČ M., *Pump absorption and temperature distribution in erbium-doped double-clad fluoride-glass fibers*, Optics Express **17**(22), 2009, pp. 19814–19822.

[17] WITKOWSKI J.S., GROBELNY A., *Ray tracing method in a 3D analysis of fiber-optic elements*, Optica Applicata **38**(2), 2008, pp. 281–294.

[18] ALLEBACH J.P., ALTMAN J.H., AMIRTHARAJ P.M., *et al.*, *Handbook of Optics*, 3rd Edition, McGraw-Hill, New York, 2010, pp. 5.1–5.29.